THE JOURNAL OF BIOLOGICAL CHEMISTRY VOL. 289, NO. 5, pp. 2801–2814, January 31, 2014


# Hepatic Apolipoprotein M (ApoM) Overexpression Stimulates Formation of Larger ApoM/Sphingosine 1-Phosphate-enriched Plasma High Density Lipoprotein*

Received for publication, July 10, 2013, and in revised form, November 24, 2013 Published, JBC Papers in Press, December 6, 2013, DOI 10.1074/jbc.M113.499913

**Mingxia Liu[‡1], Jeongmin Seo[‡1], Jeremy Allegood[§], Xin Bi[‡], Xuewei Zhu[‡], Elena Boudyguina[‡], Abraham K. Gebre[‡], Dorit Avni[§], Dharika Shah[¶], Mary G. Sorci-Thomas[‡], Michael J. Thomas[¶], Gregory S. Shelness[‡], Sarah Spiegel[§], and John S. Parks[‡¶2]**

*From the Departments of [‡]Pathology-Lipid Sciences and [¶]Biochemistry, Wake Forest School of Medicine, Winston-Salem, North Carolina 27157 and the [§]Department of Biochemistry and Molecular Biology, Virginia Commonwealth University School of Medicine, Richmond, Virginia 23298*

**Background:** ApoM overexpression in nonhepatic cells generates larger nascent HDLs.
**Results:** Hepatocyte-specific apoM transgenic mice have larger plasma HDLs and hepatocytes that generate larger nascent HDLs and increased S1P secretion.
**Conclusion:** Hepatocyte-specific apoM overexpression facilitates large apoM/S1P-enriched HDL formation by promoting large nascent HDL formation and stimulating sphingolipid synthesis and S1P secretion.
**Significance:** Hepatic apoM regulates HDL and S1P production.

**Apolipoprotein M (apoM), a lipocalin family member, preferentially associates with plasma HDL and binds plasma sphingosine 1-phosphate (S1P), a signaling molecule active in immune homeostasis and endothelial barrier function. ApoM overexpression in ABCA1-expressing HEK293 cells stimulated larger nascent HDL formation, compared with cells that did not express apoM; however, the *in vivo* role of apoM in HDL metabolism remains poorly understood. To test whether hepatic apoM overexpression increases plasma HDL size, we generated hepatocyte-specific apoM transgenic (*APOM Tg*) mice, which had an ~3–5-fold increase in plasma apoM levels compared with wild-type mice. Although HDL cholesterol concentrations were similar to wild-type mice, *APOM Tg* mice had larger plasma HDLs enriched in apoM, cholesteryl ester, lecithin:cholesterol acyltransferase, and S1P. Despite the presence of larger plasma HDLs in *APOM Tg* mice, *in vivo* macrophage reverse cholesterol transport capacity was similar to that in wild-type mice. *APOM Tg* mice had an ~5-fold increase in plasma S1P, which was predominantly associated with larger plasma HDLs. Primary hepatocytes from *APOM Tg* mice generated larger nascent HDLs and displayed increased sphingolipid synthesis and S1P secretion. Inhibition of ceramide synthases in hepatocytes increased cellular S1P levels but not S1P secretion, suggesting that apoM is rate-limiting in the export of hepatocyte S1P. Our data indicate that hepatocyte-specific apoM overexpression generates larger nascent HDLs and larger plasma HDLs, which preferentially bind apoM and S1P, and stimulates S1P biosynthesis for secretion. The unique apoM/S1P-enriched plasma HDL may serve to deliver S1P to extrahepatic tissues for atheroprotection and may have other as yet unidentified functions.**

Cardiovascular disease is the leading cause of death in developed countries. Numerous studies have observed an inverse association between plasma HDL cholesterol (HDL-C)[3] concentrations and increased cardiovascular disease risk (1). However, recent evidence suggests that HDL function, not HDL-C concentration, may best predict its atheroprotective capacity (2, 3). One function of HDL is to facilitate macrophage reverse cholesterol transport (RCT), a process by which cholesterol in arterial plaque macrophages is transported to the liver for secretion into bile and excretion in feces (4). Although RCT is presumed to be HDL's most important anti-atherogenic role, these particles also have anti-inflammatory and anti-oxidative activities and carry cardioprotective molecules (5–7). However, because our understanding of the atheroprotective roles of HDL is incomplete, additional focus on HDL function and metabolism is merited.

HDL formation initiates when the ATP-binding cassette transporter A1 (ABCA1) effluxes free cholesterol (FC) and phospholipid (PL) to lipid-free apoA-I, forming nascent HDL particles. The liver is quantitatively the most important tissue for nascent HDL formation (8). After initial assembly, nascent

* This work was supported, in whole or in part, by National Institutes of Health Grants P01HL49373 R01HL119962 (to J. S. P.), R01 HL64163 and R01 HL112270 (to M. G. S.-T.), and R37GM043880 (to S. S.). This work was also supported by American Heart Association Predoctoral Fellowship 12PRE12040309 (to M. L.).
[1] Both authors contributed equally to this work.
[2] To whom correspondence should be addressed: Dept. of Pathology/Section on Lipid Sciences, Wake Forest School of Medicine, Medical Center Blvd., Winston-Salem, NC 27157. Tel.: 336-716-2145; Fax: 336-716-6279; E-mail: jparks@wakehealth.edu.

[3] The abbreviations used are: HDL-C, HDL-cholesterol; apoM, apolipoprotein M; S1P, sphingosine 1-phosphate; *APOM Tg*, hepatocyte-specific apoM transgenic; RCT, reverse cholesterol transport; ABCA1, ATP-binding cassette transporter A1; FC, free cholesterol; PL, phospholipid; LCAT, lecithin:cholesterol acyltransferase; CE, cholesteryl ester; SR-BI, scavenger receptor class B, type I; hA-I Tg, human apoA-I transgenic; TG, triglyceride; DH-S1P, dihydrosphingosine 1-phosphate; SphK1, sphingosine kinase 1; SphK2, sphingosine kinase 2; SPTLC1, serine palmitoyltransferase long chain subunit 1; SGPP1, S1P phosphatase 1; FB1, fumonisin B1.

HDL particles undergo maturation to become spherical HDL particles via the actions of lecithin:cholesterol acyltransferase (LCAT), which increases core cholesteryl ester (CE) content (9), and phospholipid transfer protein (PLTP) (10), which transfers PL to the HDL surface. To complete the process of RCT, HDL-C is taken up by the liver, mostly via scavenger receptor class B, type I (SR-BI), for secretion into bile and excretion in feces (11).

ApoM, a 25-kDa plasma apolipoprotein, belongs to the lipocalin family and contains a small hydrophobic binding pocket (12, 13). The identity of human (NP_061974.2) and mouse apoM (NP_061286.1) is over 80%, and both contain a signal peptide anchor and hydrophobic binding pocket (13). Both the liver and kidneys produce apoM, but plasma apoM levels are likely maintained predominantly by liver expression (14). Plasma apoM mainly associates with HDL, but because of its low plasma concentration (0.9 $\mu$M), less than 5% of plasma HDL particles contain apoM (15). HDL-bound apoM can also be exchanged onto VLDL and LDL (16). *Apom* knock-out mice have a 17–21% decrease in HDL-C, whereas overexpression of human *APOM* increases HDL-C by 13–22% and protects against atherogenesis (17, 18). The antiatherogenic function of apoM has been attributed to its ability to promote pre$\beta$-HDL formation (17), stimulate cholesterol efflux from macrophage foam cells (18, 19), and increase the antioxidant activity of HDL (20). We previously demonstrated that apoM stimulates the generation of larger nascent HDL particles by HEK293 cells that overexpressed ABCA1 (21). However, whether hepatic overexpression of apoM affects plasma HDL size, composition, and function (*i.e.* RCT) *in vivo* is unknown.

In addition to its role as an HDL-binding protein, which can impact HDL metabolism, apoM is also a sphingosine 1-phosphate (S1P) carrier (22). *Apom* knock-out mice have decreased HDL-S1P, whereas *APOM* transgenic mice display an increase in HDL-S1P (22). Adenovirus-mediated overexpression of *APOM* also increases plasma apoM and S1P concentrations (23). Because S1P signaling helps maintain endothelial integrity (22, 24) and immune homeostasis (25), HDL apoM may also be atheroprotective by transporting S1P through the plasma compartment to endothelial and immune cell receptors (26). Previous studies demonstrated that tissue sources of plasma S1P include erythrocytes (27), vascular endothelial cells (28), and platelets (29, 30). Hepatocytes can also generate and secrete S1P (23, 28). Because apoM is mainly produced by the liver and its overexpression in mice increased plasma S1P levels (22), the liver may play an important role in whole body S1P distribution and homeostasis. However, to date, there are limited data regarding the extent to which hepatic apoM expression regulates hepatocyte S1P formation and secretion (23).

The goal of this study was to address unanswered questions regarding the role of hepatic apoM expression in HDL, apoM, and S1P metabolism. Based on our previous studies showing that HEK293-ABCA1-expressing cells form larger nascent HDL particles, we explored whether hepatic overexpression of apoM resulted in increased nascent and mature plasma HDL particle size and S1P content *in vivo*. We also wished to determine how hepatic apoM expression affects plasma HDL composition and the ability of HDL to promote *in vivo* macrophage RCT. Finally, we investigated the effect of hepatic apoM overexpression on hepatic sphingolipid metabolism and S1P production and secretion. Collectively, our results suggest that hepatic apoM overexpression enhances sphingolipid recycling and secretion of S1P from hepatocytes and also generates larger nascent HDLs and apoM/S1P-enriched plasma HDL particles.

## EXPERIMENTAL PROCEDURES

*Generation of Hepatocyte-specific Human APOM Transgenic (APOM Tg) Mice*—A full-length human *APOM* cDNA (GenBank™ accession number BC020683) was purchased from the National Institutes of Health mammalian gene collection, human (Invitrogen, Clone ID 4733993), and used to construct a C-terminal FLAG-tagged *APOM* cDNA as described previously (21). To create *APOM Tg* mice, MfeI and MluI sites were introduced into the 5′- and 3′-flanking ends, respectively, of C-terminal FLAG-tagged *APOM* cDNA by PCR amplification using the following primers: forward, 5′-CTGCCAATTGAAGATGTTCCACCAAATTTGGGC-3′; reverse, 5′-ACGACGCGTTCACTTGTCGTCGTCGTCCTTGTAGTCGTTATTGG-3′. Amplified cDNA was digested with MfeI and MluI and then cloned into the same sites in the pLiv-11 plasmid (31), a liver-specific transgenic expression vector (32–34). The transgene cassette containing the human apoE promoter, C-terminal FLAG-tagged human *APOM* cDNA insert, and human apoE 3′ hepatic control region was released from the plasmid construct by SpeI/SalI digestion, followed by agarose gel electrophoresis and purification of the excised gel fragment with the Elutip kit (Whatman/GE Healthcare). Pronuclear microinjection of the transgene cassette into fertilized mouse oocytes from B6D2F1 (C57BL/6×DBA/2) mice and subsequent implantation of microinjected embryos into foster mothers were conducted at the Transgenic Mouse Core Facility of Wake Forest School of Medicine. Founders were identified by PCR screening of tail genomic DNA and immunoblotting of plasma with anti-FLAG monoclonal antibody M2 (Sigma). PCR primers used to determine the presence and integrity of the transgene cassette were as follows: 5′-CACTGGCGGTTGATTGACAG-3′ and 5′-CTCACAGGCCTCTTGATTCC-3′ for the human *APOM* gene; 5′-GATGGGTTAGGAGAAGGGAGC-3′ and 5′-AGGCGGGGTCTCATTACCAAG-3′ for the human apoE promoter region; 5′-CGCCTCCACTCTGCAAGAACT-3′ and 5′-CTCTCAGAGGTCCTCTAAGCC-3′ for the human apoE hepatic control region, and 5′-GCAGATGAGTTCACTGGCTCC-3′ and 5′-AGGGCAGTTGACCTCATCGCT-3′ for the VLDL receptor, used as a load control. Upon breeding of transgenic mice with WT mice, ~50% of offspring were transgenic, confirming hemizygosity of the transgene.

*Animals*—All animal procedures were approved by the Institutional Animal Care and Use Committee of Wake Forest School of Medicine. Mice were housed in the Wake Forest School of Medicine animal facility with a 12-h light/12-h dark cycle and fed a commercial chow diet *ad libitum*. Wild-type (C57BL/6J) and homozygous human apoA-I transgenic mice on a pure C57BL/6J background (hA-I Tg) were obtained from The Jackson Laboratory (C57BL/6-Tg(APOA1)1Rub/J). *APOM Tg* mice were backcrossed into the C57BL/6J background for at least five generations. hA-I Tg/*APOM Tg* mice were generated by

crossing *APOM Tg* mice with hA-I Tg mice. All *APOM Tg* mice studied herein were compared with littermate controls.

*Plasma Lipid and Lipoprotein Quantification*—Mouse plasma was harvested by tail bleeding or cardiac puncture of anesthetized mice at sacrifice. Plasma total and free cholesterol, phospholipid, and triglyceride concentrations were measured by enzymatic assays (total cholesterol, FC, TG, and phospholipid (PC), Wako). Plasma samples were either fractionated using two Superose 6 FPLC columns (1 × 30 cm) in series (flow rate 0.5 ml/min) or by a high resolution Superose 6$^{TM}$ FPLC column (10/300GL, Amersham Biosciences; flow rate 0.5 ml/min) with an on-line cholesterol analyzer (35). Lipoprotein fractions eluted from FPLC columns were collected to determine cholesterol, TG, and PL concentrations by enzymatic assay (Wako). In some experiments, lipoprotein fractions were pooled for Western blot analysis. Lipids were extracted by the Bligh-Dyer method, and concentrations were measured by enzymatic assays (36, 37). ApoA-I concentrations were determined by ELISA (38).

*Hepatic Lipid Analysis*—Livers were perfused, snap-frozen in liquid nitrogen, and stored at −80 °C. Lipid content was quantified using detergent-based enzymatic assays as described previously (36, 37).

*In Vivo Macrophage Reverse Cholesterol Transport—In vivo* macrophage RCT assays were conducted as described by Rader and co-workers (39) with minor modifications (40). J774 mouse macrophages were radiolabeled and loaded with [$^3$H]cholesterol and acetylated LDL, respectively. Cells were then injected into the peritoneal cavity of recipient mice, and plasma samples were collected at 6, 24, and 48 h after injection. Feces were collected throughout the 48-h study. At necropsy, tissues were harvested, and $^3$H tracer levels in plasma, liver, and feces were quantified after lipid extraction and liquid scintillation counting. Aliquots of plasma were also fractionated by FPLC, and cholesterol mass and radiolabel distribution among lipoprotein fractions were quantified.

*In Vivo VLDL TG Secretion Rate Determination*—Tyloxapol (500 mg/kg body weight) was injected intravenously into 4-h fasted and anesthetized mice to block TG lipolysis acutely (41). Blood was collected before (0 min) and 30, 60, 120, and 180 min after injection for measurement of plasma triglyceride (TG) concentrations by enzymatic assay. VLDL-TG secretion rate was determined by calculating the slope of the time *versus* plasma TG concentration plot for each animal using linear regression analysis.

*Primary Hepatocyte Isolation, Nascent HDL Particle Formation, and S1P Production*—Primary hepatocytes were isolated as described previously (42) with minor modifications. After isolation from liver, hepatocytes were centrifuged at 50 × *g* for 5 min in 50% Percoll-containing Williams' media E to pellet live cells. Cells were then washed with Williams' media E before seeding in 100-mm dishes at a density of 2 × 10$^6$ cells per dish. Cells were incubated at 37 °C for 4 h before experiments were initiated. Primary hepatocytes were incubated with 10 μg/ml $^{125}$I-apoA-I (10$^5$ cpm/μg) for 24 h in serum-free DMEM using conditions described previously (43). After incubation, the conditioned media were harvested and fractionated on a Superdex-200HR FPLC column (Amersham Biosciences) eluted with 0.15 M NaCl, 0.01% EDTA, pH 7.4, at a flow rate of 0.3 ml/min. Fractions were collected and analyzed for $^{125}$I radioactivity to monitor the size distribution of nascent HDL particles.

*Quantification of Sphingolipids by Liquid Chromatography and Electrospray Ionization-Tandem Mass Spectrometry (LC-ESI-MS/MS)*—Plasma samples were freshly collected and stored in methanol before extraction. Livers were perfused via the portal vein with PBS, and liver tissues were collected and snap-frozen. HDL FPLC fractions were collected, supplemented with phosphatase inhibitors (Roche Applied Science, catalog no. 04906845001), and stored frozen. Hepatocytes from WT and *APOM Tg* mice were isolated and cultured in Williams' media E for 3 h, washed, and preincubated with serum-free DMEM for 2 h. Fresh serum-free DMEM was then replaced; hepatocytes were incubated for 6 h before media, and cells were collected for analysis. Media were centrifuged to pellet cell debris, and supernatants were harvested with addition of phosphatase inhibitors. Cells were washed with PBS and scraped off the plates in methanol. Sphingolipid content/concentration of plasma, liver, HDL, hepatocytes, and hepatocyte-conditioned medium was determined using liquid chromatography mass spectrometry. HPLC grade solvents from VWR (West Chester, PA) were used for all steps of the procedure. Extraction and quantitation of each sphingolipid species were essentially as described previously (44) using a Shimadzu LC-20 AD coupled to an ABI 4000 quadrupole/linear ion trap (QTrap, Applied Biosystems, Foster City, CA) operating in a triple quadrupole mode as described previously (44).

In some experiments, S1P concentrations in plasma and FPLC-isolated plasma lipoprotein fractions were also measured essentially as described by Berdyshev *et al.* (45) using 25-μl aliquots of mouse plasma containing 50 pmol of $C_{17}$S1P as an internal standard. After extraction and derivatization, bisacetylated S1P was analyzed on a YMC-Pack ODS-AQ column (100 × 1.0 mm inner diameter, 3-μm particle size) and detected using a ThermoFinnigan TSQ Quantum Discovery Max Triple Quadrupole mass spectrometer in negative ion mode. Bisacetylated sphingolipids were eluted using the following gradients: 2 min hold of solvent A/solvent B (50:50), ramp to 100% solvent B over 0.1 min, hold at 100% solvent B for 8.5 min and then regenerate the column with solvent A/solvent B (50:50) for 30 min with the following settings: ion spray voltage −3000 V, ion transfer capillary temperature 200 °C, collision gas 1 millitorr of argon with a collision energy of 11 V. Multiple reaction monitoring transitions monitored were $C_{17}$S1P *m*/*z* 448/388 and S1P *m*/*z* 462/402.[4]

*Analysis of Hepatocyte S1P Synthesis and Secretion*—S1P synthesis from radiolabeled sphingosine was measured as described previously (47). Primary hepatocytes were isolated from WT and *APOM Tg* mice, seeded in 35-mm dishes, and incubated in serum-free media for 2 h at 37 °C before addition of 0.225 μCi of [$^3$H]sphingosine (PerkinElmer Life Sciences) and 1.5 mM sphingosine (Cayman Chemical) per dish for 10 min to radiolabel cells. Medium was then switched to fresh serum-free DMEM, and cells were incubated at 37 °C for 2 h

[4] K. L. Brzoza-Lewis, E. L. Lyons, M. Zabalawi, A. J. Wilhelm, B. E. Fulp, D. P. Shah, J. S. Owen, M. Gerelus, J. Barlic-Dicen, M. J. Thomas, and M. G. Sorci-Thomas, submitted for publication.

before media and cells were collected for differential lipid extraction (47). Cell and media [$^3$H]S1P radiolabels were quantified by liquid scintillation spectroscopy after extraction. Data are presented as [$^3$H]S1P/total $^3$H radiolabel × 100% in cells or media, normalized to cellular PL content as measured by phosphorus assay (48).

*Myriocin and Fumonisin B1 Treatment*—Primary hepatocytes were isolated and seeded for 2 h before they were washed and incubated with serum-free media for 2 h. Myriocin (Sigma) dissolved in methanol and fumonisin B1 (Sigma) dissolved in ethanol were added to hepatocytes at a final concentration of 10 and 25 $\mu$M, respectively, and incubated for 6 h before media were collected and supplemented with phosphatase inhibitors. Control dishes were incubated with the appropriate vehicle. Cells were washed and collected in methanol. Both cells and media were subjected to LC-ESI-MS/MS analysis. Replicate dishes in each group were used to determine protein content by BCA assay.

*Western Blotting*—Proteins were fractionated by SDS-PAGE and transferred to a nitrocellulose membrane (Schleicher & Schuell) (250 mA, 2 h). Membranes were blocked with 5% nonfat dry milk in TBST buffer, incubated with primary antibody at 4 °C overnight, washed three times, and then incubated with secondary antibody for 1 h at room temperature. Blots were incubated with SuperSignal West Pico chemiluminescence substrate (Pierce) and visualized with a Fujifilm LAS-3000 camera. Antibodies used for Western blots included the following: anti-FLAG monoclonal antibody M2 (Sigma); anti-apoE and anti-LCAT (generated in-house); anti-mouse apoM (Lifespan); anti-human and mouse apoM (Abcam); anti-mouse apoA-I (Biodesign); anti-GAPDH (Sigma), and HRP-conjugated anti-mouse and anti-rabbit secondary antibodies (GE Healthcare). Band intensities were quantified using MultiGauge software (Fujifilm).

*Gene Expression Analysis*—RNA was isolated from liver and hepatocytes using TRIzol (Invitrogen) and reverse-transcribed into cDNA using Omniscript RT kit (Qiagen). Expression levels were analyzed by quantitative real time PCR (49). Primers used for indicated gene expression are: *GAPDH,* forward, TGTGTCCGTCGTGGATCTG, and reverse, CCTGCTTCACCACCTTCTTGAT; *SPTLC1*, forward, AGTGGTGGGAGAGTCCCTTT, and reverse, CAGTGACCACAACCCTGATG; *SPHK2,* forward, CGGATGCCCATTGGTGTCCTC, and reverse, TGAGCAACAGGTCAACACCGAC; *SGPP1,* forward, GAAGTGGTGCTGGAATTGCATGTG, and reverse, GCAATATGGCTTTTCCAAACAGAGTCA; acid *SMase*, forward, ATGCCCTTCACACCCTAAGAA, and reverse, AGCAGGATCTGTGGAGTTGA; *SR-BI*, forward, GGCTGCTGTTTGCTGCG, and reverse, GCTGCTTGATGAGGGAGGG.

*Statistics*—Results were reported as mean ± S.E. Two-tailed Student's *t* tests were used to detect statistically significant differences between wild-type and *APOM Tg* mice. Two-way analysis of variance and the Bonferroni post hoc test were used to analyze data from myriocin and fumonisin B1 inhibition experiments. A $p$ value $<0.05$ was considered statistically significant. Statistical analyses were performed with GraphPad Prism software.

## RESULTS

*Generation of Hepatocyte-specific Human APOM Transgenic Mice*—Hepatocyte-specific APOM transgenic (*APOM Tg*) mice were generated using the pLiv11 vector (32–34). PCR of mouse tail genomic DNA was used to identify transgenic positive mice. To estimate the level of overexpression of human apoM, WT and *APOM Tg* mouse plasma were analyzed by Western blot analysis using an antibody (Abcam) that detects both mouse and human apoM (Fig. 1*A*). The mass of apoM observed in 2 $\mu$l of WT and Tg mouse plasma is consistent with ~3–5-fold overexpression of apoM in the Tg mice.

*Quantification of Plasma and Liver Lipids in APOM Tg Mice*—We examined plasma lipid and lipoprotein cholesterol concentrations in *APOM Tg* mice in both WT and human apoA-I Tg (hA-I) backgrounds. Two different backgrounds were examined because WT mice have relatively uniformly sized HDL particles, whereas hA-I Tg mice have polydispersed HDL subfractions that are similar in size to human plasma HDL particles (50). In both WT and hA-I backgrounds, male *APOM Tg* mice had significantly increased plasma total cholesterol (24% increase in WT and 10% increase in hA-I background), PL (29% increase in WT and 19% increase in hA-I background), and triglyceride (TG) (4.5-fold increase in WT and 6.7-fold increase in hA-I background) concentrations relative to their non-apoM transgenic counterparts (Fig. 1*B*). Plasma FC (WT, 35.55 ± 0.84 *versus APOM Tg*, 49.14 ± 4.17 mg/dl, $p < 0.05$) and CE (WT, 111.2 ± 2.5; *APOM Tg*, 130.2 ± 5.8 mg/dl, $p < 0.05$) were both increased in *APOM Tg* mice, relative to the WT control. FPLC fractionation of plasma revealed that the increased plasma cholesterol level in *APOM Tg* mice was mostly attributed to increased plasma VLDL (7.6-fold increase in WT and 15.8-fold increase in hA-I background) and LDL concentrations (no increase in WT and 1.7-fold increase in hA-I background) (Fig. 1*C*). In contrast, HDL-C did not differ between *APOM Tg* mice and their control counterparts in both backgrounds (Fig. 1*C*). We observed a similar lipid and lipoprotein phenotype in female mice (data not shown).

Whole plasma apoB concentrations were also increased in *APOM Tg* mice, suggesting an increase in plasma apoB-containing lipoproteins (Fig. 2, *A* and *B*). To determine whether liver-specific overexpression of human apoM increased hepatic VLDL-TG secretion, we acutely inhibited intravascular TG lipolysis using a detergent block procedure and observed similar rates of plasma TG accumulation in WT and *APOM Tg* mice (Fig. 2, *C* and *D*), suggesting that hepatic VLDL TG secretion was not altered by overexpression of human apoM. Thus, in agreement with a previous study (51), increased plasma VLDL-C and TG likely resulted from delayed VLDL catabolism. In contrast to plasma values, hepatic levels of FC, CE, and TG were similar in WT and *APOM Tg* mice (data not shown), except for a significant decrease in hepatic CE in male *APOM Tg* mice (WT, 0.52 ± 0.07 *versus APOM Tg* 0.27 ± 0.07 $\mu$g per mg liver weight, $p < 0.05$).

*APOM Tg Mice Generated Larger Plasma HDLs Enriched in CE, ApoE, LCAT, and ApoM*—We previously reported that apoM overexpression in a nonhepatic cell line (HEK293-ABCA1) generated larger nascent HDL particles (21). To deter-

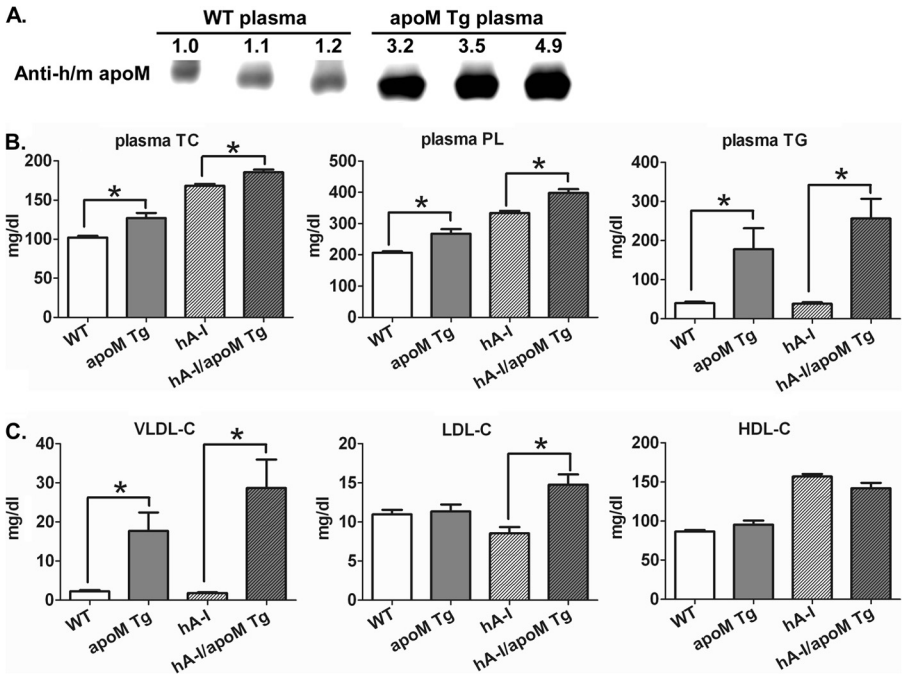


FIGURE 1. **Lipid and lipoprotein characteristics of *APOM Tg* mice.** *A,* Western blot analysis of 2 $\mu$l of WT and *APOM Tg* mouse plasma using an antibody that detects both mouse and human apoM. Band intensities were quantified using MultiGauge software. The intensity of the least intense band for WT and *APOM Tg* plasma was set to 1, and other bands were normalized to its intensity and are shown *above* the bands. *B,* plasma total cholesterol (*TC*), phospholipid (*PL*), and triglycerides (*TG*) from male mice were analyzed by enzymatic assays. *C,* plasma lipoproteins were fractionated by FPLC, and cholesterol concentration in VLDL, LDL, and HDL was determined by enzymatic assays. *B* and *C*, $n = 13$, 9, 11, and 12 for WT, *APOM Tg*, hA-I, and hA-I/*APOM Tg* mice, respectively. *, $p < 0.05$, *APOM Tg* mice *versus* their control (WT or hA-I) counterparts. *hA-I* = human apoA-I transgenic mouse.

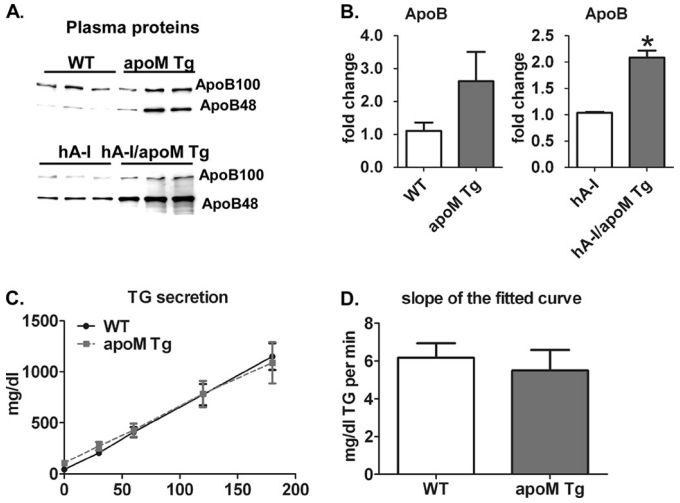


FIGURE 2. ***APOM Tg* and WT mice have comparable hepatic TG secretion.** *A,* plasma samples from mice of the indicated genotypes were Western-blotted for apolipoprotein B. *B,* Western blot results were quantified using MultiGauge software. Total apoBs from apoB100 and apoB48 were calculated, normalized to total apoB in WT sample on the *1st lane* as fold change, and plotted; *, $p < 0.05$. *C* and *D,* mice fasted for 4 h were retro-orbitally injected with tyloxapol (500 mg/kg) to block TG lipolysis acutely. Blood was collected before injection (0) and 30, 60, 120, and 180 min after injection. *C,* plasma TG levels at each time point were determined by enzymatic assay and plotted; $n = 5$. *D,* slope of the line of best fit for each mouse was calculated by linear regression analysis using GraphPad Prism software; *, $p < 0.05$.

mine whether liver-specific overexpression of human apoM increased HDL particle size *in vivo*, we studied plasma lipoprotein distribution by FPLC size exclusion chromatography. Interestingly, in both WT and hA-I backgrounds, HDL from *APOM Tg* mice eluted from the FPLC column at an earlier position relative to their WT counterparts, suggesting increased HDL particle size (Fig. 3*A*). To further explore this, we measured the lipid content of the FPLC-isolated HDL and normalized the results to apoA-I content, as determined by ELISA. As shown in Table 1, HDLs from *APOM Tg* mice contained significantly more CE and PL per apoA-I molecule, likely contributing to the increased HDL size in *APOM Tg* mice. The HDL ratio of surface lipid and protein to core lipids (FC + PL + apoA-I)/CE was significantly decreased in *APOM Tg versus* WT mice (Table 1), also agreeing with increased HDL size in *APOM Tg* mice. Finally, we examined the protein composition of the FPLC-isolated HDL fractions by Western blot analysis. In both genetic backgrounds, *APOM Tg* mice had HDLs with more apoE and LCAT than their WT counterparts (Fig. 3, *B* and *C*). Endogenous mouse *apom* expression was lower in *APOM Tg* mice in both backgrounds (Fig. 3, *B* and *C*), presumably due to displacement by the more abundant human apoM. In general, apoE-containing HDLs are larger than non-apoE-containing HDL particles (52). The enrichment of LCAT on HDLs from *APOM Tg* mice likely leads to enhanced conversion of FC to CE, resulting in increased HDL size and CE content in *APOM Tg* mice.

*ApoM Predominantly Associates with Larger Sized HDL*—Because we observed a similar increase in HDL size in *APOM Tg* mice for both WT and hA-I backgrounds, all subsequent studies were performed using *APOM Tg* mice in the WT background. To determine the relationship between HDL particle size and apoM content, we examined apoM distribution across HDL fractions eluted from an FPLC column. The cholesterol distribution for WT and *APOM Tg* mouse plasma fractionated by FPLC is shown in Fig. 4*A*; the distribution of mouse and human apoM and mouse apoA-I, determined by Western blot analysis, is shown in Fig. 4*B*. Using mouse apoA-I as a protein

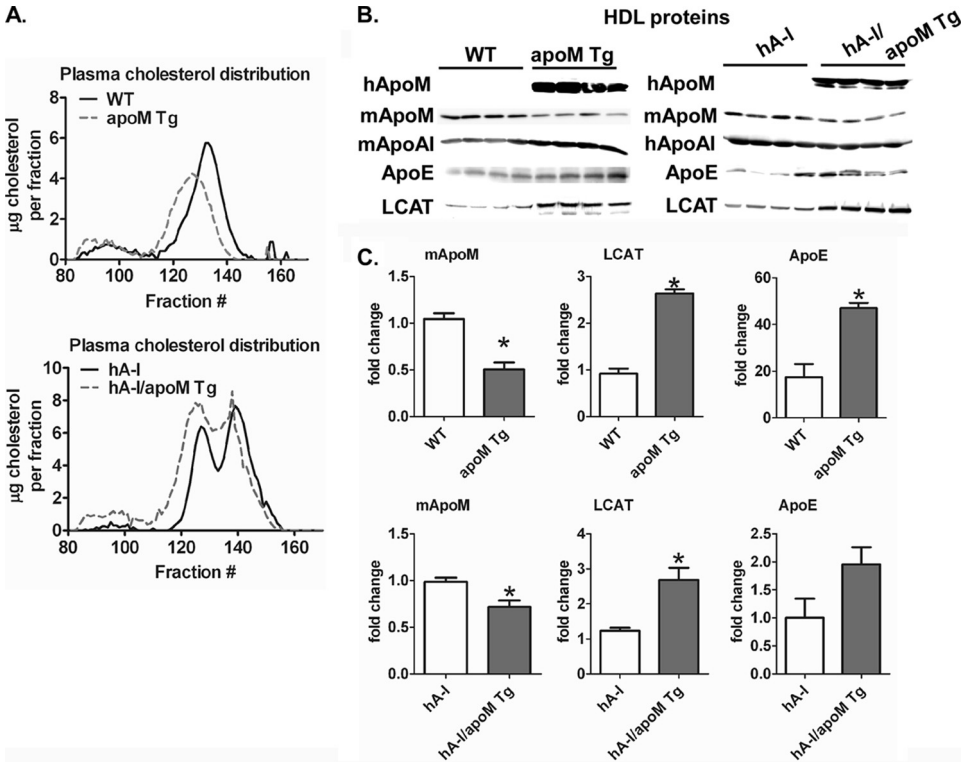


FIGURE 3. ***APOM Tg* mice have larger HDL enriched in LCAT, apoM, and apoE.** *A,* representative lipoprotein cholesterol distribution profiles were acquired from high resolution FPLC size fractionation of equal volumes of plasma from mice of the indicated genotypes. *B,* FPLC fractionated HDL (*A*) was pooled (fractions 110–150) and an equivalent fraction of each HDL peak was TCA-precipitated and subjected to SDS-PAGE and Western blot analysis. *h,* human; *m,* mouse. *C,* quantification of Western blot band intensities in *B* was performed with MultiGauge software. Fold change of each protein is expressed relative to the expression levels in WT samples. *, $p < 0.05$.

**TABLE 1**

**Chemical composition of HDL from WT and APOM Tg mice**

FPLC-fractionated HDL (Fig. 2*A*) was pooled (fractions 110–150), and an equivalent fraction of each HDL peak was subjected to lipid extraction. TC, FC, and PL compositions of HDLs from WT and *APOM Tg* mice were analyzed by enzymatic assays. Esterified cholesterol (EC) was calculated from total cholesterol (TC) and FC. Mouse apoA-I levels were measured by ELISA. Values are means ± S.D. ($n = 7$ and 5 for WT and *APOM Tg* mice, respectively).

| | TC | PL | EC | FC | EC/FC | TC/PL | (FC + PL + apoA-I)/CE |
|---|---|---|---|---|---|---|---|
| | *mg/mg apoA-I* | *mg/mg apoA-I* | *mg/mg apoA-I* | *mg/mg apoA-I* | *mg/mg* | *mg/mg* | *mg/mg* |
| WT | 1.8 ± 0.4 | 4.3 ± 0.7 | 1.3 ± 0.3 | 0.5 ± 0.1 | 2.4 ± 0.2 | 0.4 ± 0.0 | 2.7 ± 0.2 |
| *APOM Tg* | 2.3 ± 0.2 | 5.1 ± 0.4 | 1.7 ± 0.2 | 0.6 ± 0.1 | 2.9 ± 0.5 | 0.4 ± 0.0 | 2.4 ± 0.3 |
| *p* | 0.042 | 0.047 | 0.02 | 0.508 | 0.014 | 0.271 | 0.042 |

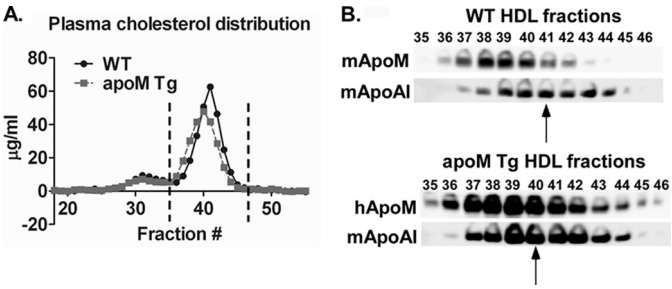


FIGURE 4. **ApoM predominantly associates with large HDL.** *A,* equivalent amount of plasma from WT and *APOM Tg* mice was fractionated using FPLC, and cholesterol concentrations were determined using enzymatic assay. *B,* HDL fractions from 35–46 (*dashed vertical lines*) were collected and TCA-precipitated for Western blot analysis of mouse and human apoM and mouse apoA-I. The *arrows* identify the fractions corresponding to the peak of HDL cholesterol.

marker of HDL particle size distribution, we observed that mouse and human apoM distribution was shifted to earlier eluting fractions relative to apoA-I, demonstrating that both endogenous mouse apoM and transgenic human apoM preferentially associate with larger HDL particles.

*Primary Hepatocytes from APOM Tg Mice Produce Larger Nascent HDL Particles*—To determine whether increased plasma HDL size in *APOM Tg* mice resulted from assembly of larger nascent HDL by hepatocytes, we isolated primary hepatocytes from WT and *APOM Tg* mice and examined nascent HDL formation by incubating hepatocytes with $^{125}$I-apoA-I for 24 h, followed by size exclusion chromatography. As shown in Fig. 5, hepatocytes from *APOM Tg* mice generated a similar number of small nascent HDL particles but relatively more particles of larger sizes as compared with WT mice. This agreed with our previous finding using the nonhepatic HEK293-ABCA1-expressing cell line, which showed that apoM overexpression increased nascent HDL particle size (21). Because nascent HDL particles undergo maturation by LCAT and plasma HDLs from *APOM Tg* mice were enriched in LCAT (Fig. 3*B*), it appears that HDL generated by *APOM Tg* mouse hepatocytes may better recruit LCAT, thereby leading to production of

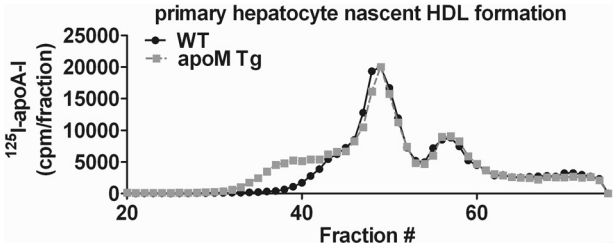


FIGURE 5. **Primary hepatocytes from *APOM Tg* mice generated larger nascent HDL.** Primary hepatocytes from WT and *APOM Tg* mice were isolated and incubated with $^{125}$I-apoA-I (10 $\mu$g/ml) in serum-free DMEM for 24 h. Media were collected and fractionated using a Superdex-200 FPLC column, and the radiolabel in each fraction was quantified.

larger sized CE-enriched plasma HDLs. The increase in HDL particle size is probably not attributable to decreased HDL catabolism, because hepatic levels of SR-BI mRNA and protein levels of SR-BI and LDL receptor-related protein (data not shown), both of which are involved in HDL catabolism (53–55), were similar in both genotypes. Additionally, HDL isolated from *APOM Tg* and WT mice had similar protein binding capacity (215.3 ± 29.7 *versus* 232.4 ± 21.3 ng of HDL protein/2 h per mg of cell protein) and HDL cholesterol ester uptake (12.9 ± 0.3% *versus* 13.6 ± 0.3%) in IdA cells overexpressing SR-BI (56). Overall, our data suggest that larger nascent HDL particles generated from hepatocytes overexpressing apoM lead to generation of larger mature plasma HDL.

*Increased HDL Size in APOM Tg Mice Did Not Promote in Vivo Macrophage Reverse Cholesterol Transport*—A previous study showed that apoM-enriched HDL from *APOM Tg* mice increased cholesterol efflux from macrophage foam cells compared with WT mouse HDL, although macrophage RCT was not correspondingly increased *in vivo* (19). However, in this previous study, no increase in plasma HDL size was reported. To determine whether the larger plasma HDL particles observed in our *APOM Tg* mice increased RCT, [$^3$H]cholesterol-loaded macrophages were injected into the peritoneal cavity of WT and *APOM Tg* mice, followed by periodic blood sampling. Mice were sacrificed 48 h after injection, and liver, plasma, and feces were collected for [$^3$H]cholesterol quantification. At all times up to 48 h after injection, *APOM Tg* and WT mice had comparable levels of plasma [$^3$H]cholesterol radiolabel (Fig. 6*A*), even though the FPLC distribution of radiolabel among plasma lipoproteins revealed more radiolabel in larger HDL of *APOM Tg versus* WT mice (Fig. 6*B*). These data suggest a similar ability of plasma from WT and *APOM Tg* mice to efflux macrophage-radiolabeled cholesterol. Furthermore, the radiolabel in liver (Fig. 6*C*) and feces (Fig. 6*D*) was similar for WT and *APOM Tg* mice, suggesting that larger apoM-enriched HDL particles in *APOM Tg* mice do not enhance *in vivo* macrophage RCT.

*Large HDL in APOM Tg Mice Preferentially Transport S1P*—Because recent studies suggested that S1P is transported in plasma by apoM, and its plasma concentration is increased in apoM transgenic mice and decreased in apoM knock-out mice (22, 57), we explored the extent to which the larger HDL particles in our *APOM Tg* mice increased S1P levels. Plasma S1P concentrations were increased ~5-fold in *APOM Tg* mice (~3.5 $\mu$M) *versus* WT (~0.7 $\mu$M) (Fig. 7*A*). Dihydrosphingosine

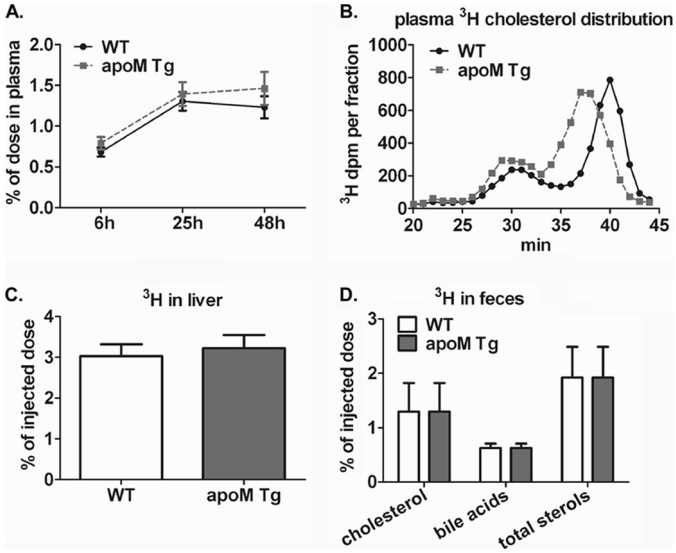


FIGURE 6. ***APOM Tg* and WT mice have similar *in vivo* macrophage reverse cholesterol transport.** J774 macrophages loaded with acetylated LDL and [$^3$H]cholesterol were injected into the peritoneal cavity of WT and *APOM Tg* mice ($2.9 \times 10^6$ dpm in 500 $\mu$l of cell suspension/mouse; $n = 7$ for each genotype). Blood samples were collected as indicated, and mice were sacrificed 48 h after injection for terminal blood and liver harvest; feces were collected throughout the 48-h study. Data were normalized to the percentage of injected dose. *A,* plasma radioactivity. *B,* equivalent volumes of terminal plasma were fractionated by FPLC, and radioactivity in each fraction was quantified. *C,* liver lipids were extracted as described (41), and lipid radioactivity was quantified. *D,* cholesterol and bile acids were extracted from feces, and radioactivity was quantified.

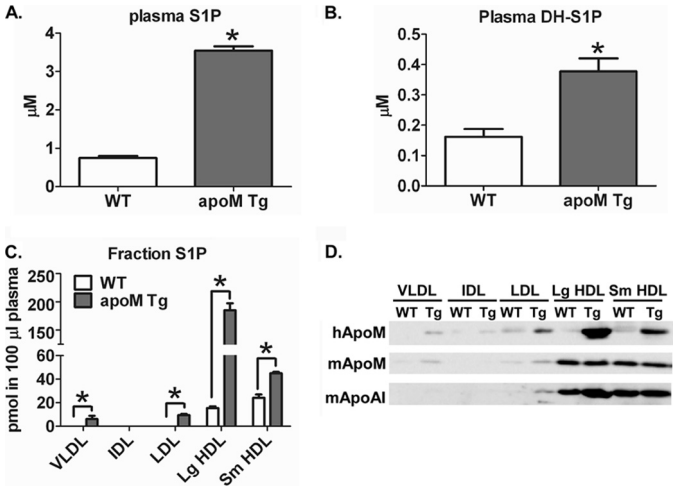


FIGURE 7. ***APOM Tg* mice have increased S1P in large sized HDLs.** Plasma S1P (*A*) and DH-S1P (*B*) in WT and *APOM Tg* mice were quantified by mass spectrometry. $n = 3$ for each genotype, *, $p < 0.05$. *C,* plasma lipoproteins were fractionated by FPLC, and aliquots of the indicated lipoprotein fractions were quantified for S1P using mass spectrometry; results were normalized to 100 $\mu$l of plasma. $n = 3$ for each genotype; *, $p < 0.05$. *D,* lipoprotein fractions from equivalent volumes of plasma were TCA-precipitated, subjected to SDS-PAGE, and Western-blotted for human and mouse apoM and mouse apoA-I. *Lg,* large. *Sm,* small.

1-phosphate (DH-S1P), a product of dihydrosphingosine phosphorylation by sphingosine kinases, was also increased ~2-fold in *APOM Tg* mouse plasma (Fig. 7*B*). S1P was significantly increased in plasma VLDL, LDL, and HDL of *APOM Tg* mice, but the largest increase and the predominant lipoprotein fraction containing S1P was large HDL (Fig. 7*C*). Large HDL was also most enriched in apoM (Figs. 4 and 7*D*). Collectively, these

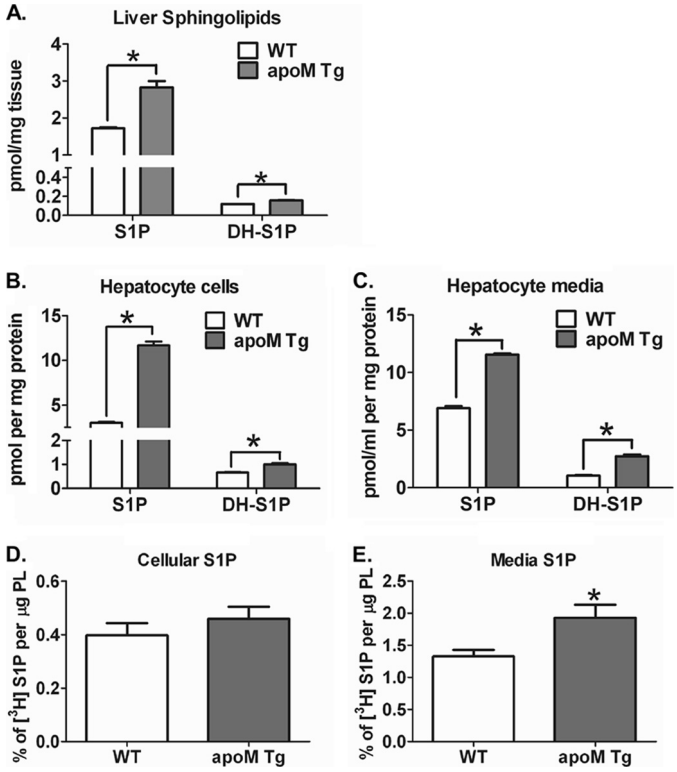


FIGURE 8. ***APOM Tg* mice have increased hepatic S1P production and secretion.** *A,* liver tissues were subjected to lipid extraction, and S1P and DH-S1P were analyzed by LC-ESI-MS/MS. *B* and *C,* hepatocytes from WT and *APOM Tg* mice were incubated in 1 ml of serum-free medium for 6 h. Lipids were extracted from cells (*B*) and media (*C*), and sphingolipids were analyzed by LC-ESI-MS/MS. *A–C,* data were normalized to liver or cellular protein content; $n = 3$ for each genotype; *, $p < 0.05$. *D* and *E,* primary hepatocytes were isolated from WT and *APOM Tg* mice and incubated in serum-free media for 2 h at 37 °C before addition of 0.225 μCi of [$^3$H]sphingosine and 1.5 mM sphingosine for 10 min to radiolabel cells. Medium was replaced with serum-free DMEM, and cells were incubated at 37 °C for 2 h before media and cells were collected for lipid extraction. Cell (*D*) and media (*E*) [$^3$H]S1P radiolabel were quantified by liquid scintillation spectroscopy after differential extraction (48). Data are presented as [$^3$H]S1P/total $^3$H radiolabel × 100%, normalized to cellular PL content measured by phosphorus assay. $n = 3$/genotype; *, $p < 0.05$.

data suggest that hepatocyte-specific apoM overexpression generates larger size HDL particles that appear optimal for binding both apoM and S1P.

*APOM Tg Mice Have Increased Hepatic S1P Levels and Secretion*—Because *APOM Tg* mice had increased plasma S1P, we examined the contribution of hepatic S1P and its secretion to this observation. There were significant increases in liver S1P (1.6-fold) and DH-S1P (1.3-fold) in *APOM Tg* mice *versus* WT (Fig. 8*A*). Although red blood cells, vascular endothelial cells, and platelets are believed to be the major sources of plasma S1P (27, 28), the contribution of S1P produced by hepatocytes is still not clear. Interestingly, there were significantly greater levels of S1P (3.9-fold) and DH-S1P (1.5-fold) in hepatocytes isolated from *APOM Tg* mice than in WT hepatocytes (Fig. 8*B*), whereas levels of their precursors sphingosine and DH-sphingosine were not significantly changed (data not shown). Next, we tested the effect of apoM overexpression on S1P secretion from primary hepatocytes. In agreement with the notion that apoM is a physiological carrier of S1P (22), larger amounts of S1P (1.6-fold) and DH-S1P (2.6-fold) were secreted from cultured primary hepatocytes overexpressing apoM compared with their WT counterparts (Fig. 8*C*), whereas sphingoid bases levels in the medium were similar (data not shown). To further examine the effect of apoM overexpression on hepatocyte S1P synthesis and secretion, primary mouse hepatocytes were incubated with [$^3$H]sphingosine. Although both WT and *APOM Tg* hepatocytes produced similar amounts of [$^3$H]S1P (Fig. 8*D*), *APOM Tg* hepatocytes secreted significantly more [$^3$H]S1P (Fig. 8*E*), further supporting the notion that apoM overexpression enhances secretion of S1P from hepatocytes.

*Increased Sphingolipid Content in Hepatocytes from APOM Tg Mice*—Hepatocytes from *APOM Tg* mice also had significantly increased cellular ceramide and sphingomyelin content compared with those from WT mice (Fig. 9*A*). The major ceramide species in hepatocytes are the very long chain ceramides, C22:0, C24:1, and C24:0, followed by the long chain C16 species (Fig. 9*B*). All of these ceramide species were increased to similar extents by overexpression of apoM, suggesting that cellular ceramide content does not increase because of changes in activity of specific ceramide synthases with different fatty acyl-CoA specificity. In contrast, ceramide and sphingomyelin content in the media of hepatocytes overexpressing apoM was decreased (Fig. 9*C*). Taken together, these results suggest that apoM overexpression in hepatocytes specifically promotes the secretion of S1P and DH-S1P but not other sphingolipid species. In addition, comparable levels of ceramide and sphingomyelin were found in plasma and HDL fractions from *APOM Tg* and WT mice (data not shown).

Sphingosine kinase 1 and 2 (SphK1 and SphK2) catalyze the production of S1P and DH-S1P from sphingosine and DH-sphingosine, respectively (Fig. 9*D*). To determine whether SphK1 and SphK2 were up-regulated in *APOM Tg* mice, leading to increased cellular S1P and DH-S1P levels in hepatocytes, we measured mRNA expression in liver and primary hepatocytes. Expression of SphK1 was barely detectable in liver and hepatocytes (Fig. 9, *E* and *F*), whereas SphK2 was slightly up-regulated in liver (Fig. 9*E*), but not in primary hepatocytes (Fig. 9*F*), from *APOM Tg* mice. SphK2 protein expression was similar in WT and *APOM Tg* mouse primary hepatocytes (data not shown). Furthermore, the major hepatocyte sphingosine kinase activity was SphK2, with minimal SphK1 activity (Fig. 9*G*). Although there was no apparent difference in SphK2 protein expression, its activity was slightly but significantly increased (29%) in hepatocytes from *APOM Tg* mice. We also analyzed liver expression of other key enzymes involved in generation or breakdown of S1P (Fig. 9*E*), including SPTLC1, acid sphingomyelinase, and SGPP1; only acid sphingomyelinase was slightly increased. Overall, these data indicate that there are no major changes in the expression of genes involved in sphingolipid metabolism in *APOM Tg* mice.

*Ceramide Synthase Inhibition Induces Cellular Levels, but Not Secretion, of S1P and DH-S1P in Hepatocytes from APOM Tg Mice*—Ceramide, the precursor of sphingosine and S1P, is produced in cells by *de novo* biosynthesis, which is initiated by the condensation of serine with palmitoyl-CoA by serine palmitoyltransferase or by recycling of sphingosine via a salvage pathway (Fig. 9*D*). Dihydrosphingosine, but not sphingosine, is an intermediate in the *de novo* biosynthesis pathway. To examine

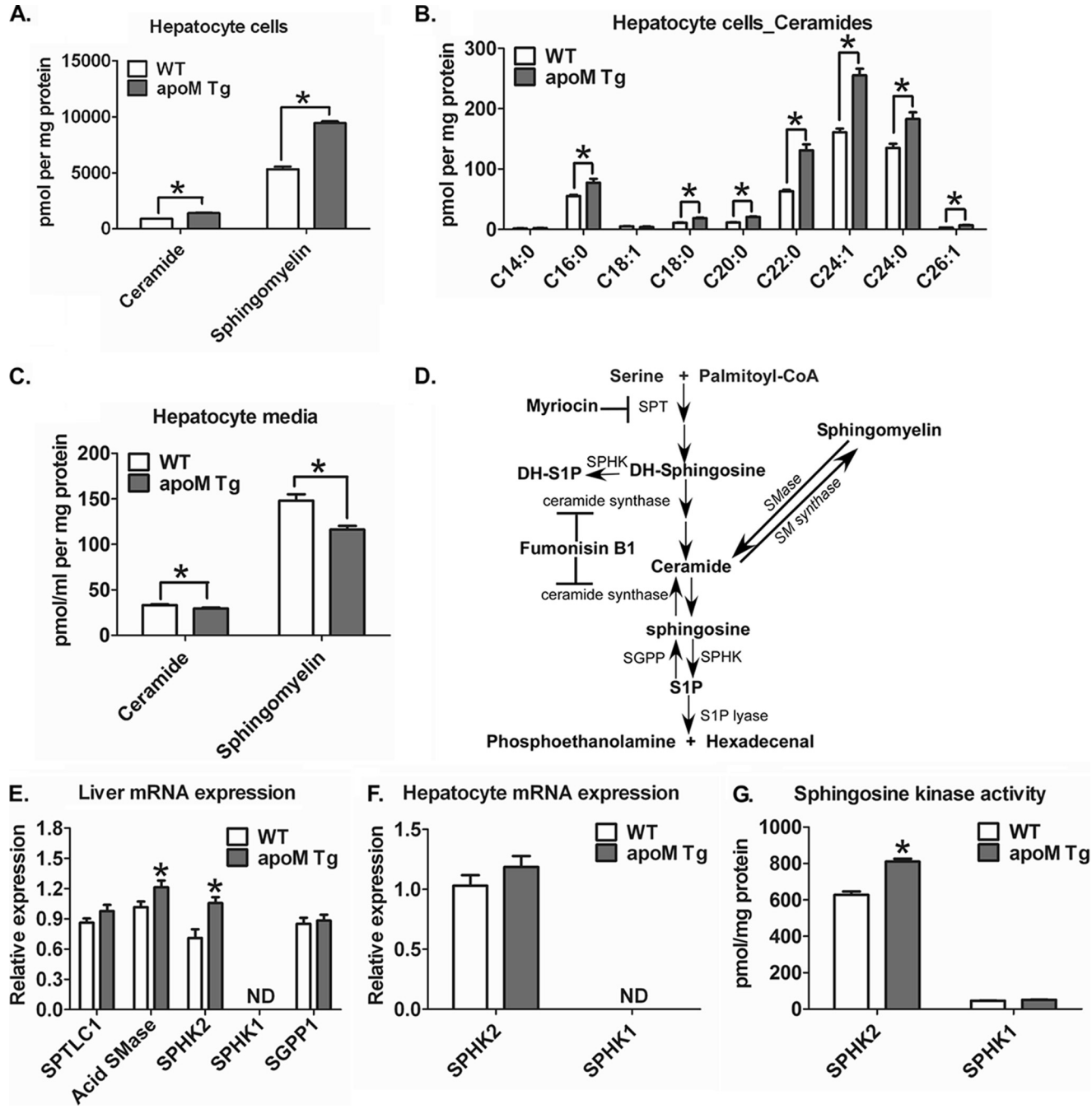


FIGURE 9. **Hepatocytes from *APOM Tg* mice have increased sphingolipid content.** Lipids were extracted from hepatocytes (*A* and *B*) and media (*C*) as described in Fig. 7*B,* and ceramide and sphingomyelin content was quantified by LC-ESI-MS/MS. *B,* different chain length species of ceramide are shown; *numbers* indicate chain length followed by the number of double bonds in the fatty acid. Data were normalized by cellular protein content; *, $p < 0.05$. *D,* simplified pathway of sphingolipid synthesis. *SPT,* serine palmitoyltransferase; *SPHK,* sphingosine kinase; *SGPP,* S1P phosphatase; *S1P,* sphingosine 1-phosphate; *SMase*, sphingomyelinase. Myriocin is an inhibitor of *de novo* (*i.e.* SPT) sphingolipid synthesis, and fumonisin B1 is an inhibitor of ceramide synthase (*i.e.* sphingosine *N*-acyltransferase). *E* and *F,* RNA was isolated from liver (*E*) and primary hepatocytes (*F*) of WT and *APOM Tg* mice, transcribed into cDNA, and quantified by quantitative real time PCR. *E,* expression of serine palmitoyltransferase long chain 1 (*SPTLC1*), acid sphingomyelinase (*acid SMase*), sphingosine kinase 2 (*SphK2*), sphingosine kinase 1 (*SphK1*), and sphingosine 1-phosphate phosphatase 1 (*SGPP1*), normalized to GAPDH. $n = 6$/genotype. *, $p < 0.05$. *F,* expression of primary hepatocyte SphK1 and SphK2 mRNA, normalized to GAPDH. $n = 4$ for each genotype. *ND,* not detected. *G,* activities of sphingosine kinase 1 and 2 were measured in hepatocytes from WT and *APOM Tg* mice following procedures described in Ref. 46. $n = 9$ for each genotype. *, $p < 0.05$.

the pathways involved in the generation of increased levels of S1P and long chain ceramides in apoM-overexpressing hepatocytes, we used myriocin (ISP-1), a specific inhibitor of serine palmitoyltransferase (58), and fumonisin B1 (FB1), an inhibitor of CoA-dependent dihydroceramide/ceramide synthases (59). Myriocin treatment did not significantly decrease cellular ceramide levels in WT and apoM-overexpressing hepatocytes (Fig. 10*A*), yet, as expected, it did decrease levels of dihydroceramides (Fig. 10*B*) and dihydrosphingosine (data not shown). Although S1P levels in hepatocytes overexpressing apoM were slightly decreased by myriocin treatment (Fig. 10*C*), this decrease did not affect secretion of S1P or DH-S1P (Fig. 10*D*).

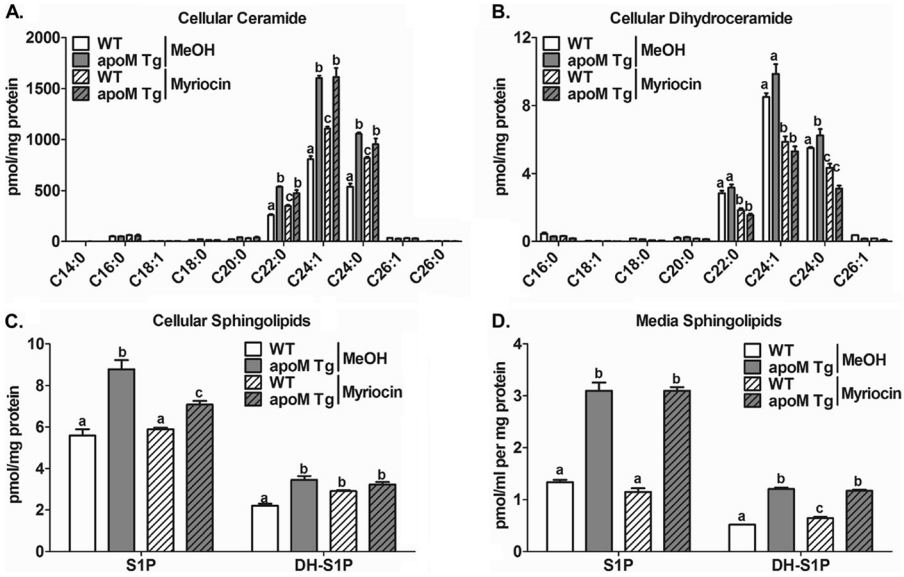


FIGURE 10. **Effect of myriocin on sphingolipid biosynthesis in hepatocytes overexpressing apoM.** Primary hepatocytes were isolated from WT and *APOM Tg* mice and treated with vehicle or 10 $\mu$M myriocin for 6 h in 1 ml of serum-free media. Lipids were extracted from cells (*A–C*) and media (*D*) and the indicated sphingolipids determined by LC-ESI-MS/MS. Different chain length species of ceramide (*A*) and dihydroceramides (*B*) are shown; *numbers* indicate chain length followed by the number of double bonds in the fatty acid. *Unlike letters* in the figure indicate significant differences ($p < 0.05$) between genotypes or between vehicle and myriocin treatment.

Collectively, these data suggest that *de novo* sphingolipid synthesis only plays a minor role in elevating cellular ceramide and S1P in *APOM Tg* hepatocytes and does not influence secretion of S1P or DH-S1P.

In agreement with previous studies (60), FB1, which inhibits all six ceramide synthases, reduced ceramide levels (Fig. 11*A*). Importantly, it also reduced cellular ceramide levels in apoM-overexpressing hepatocytes (Fig. 11*A*). Decreases in cellular ceramides were accompanied by increased levels of sphingosine and dihydrosphingosine (data not shown), as well as their phosphorylated forms, S1P and DH-S1P (Fig. 11*B*). These data suggest that recycling of sphingosine to the ceramide biosynthetic pathway is enhanced by apoM overexpression. However, although FB1 induced a large increase in cellular S1P and DH-S1P, it had no effect on their secretion into the medium, even in hepatocytes overexpressing apoM (Fig. 11*C*). Taken together, these results suggest that apoM is rate-limiting in mobilizing cellular S1P (and DH-S1P) for secretion.

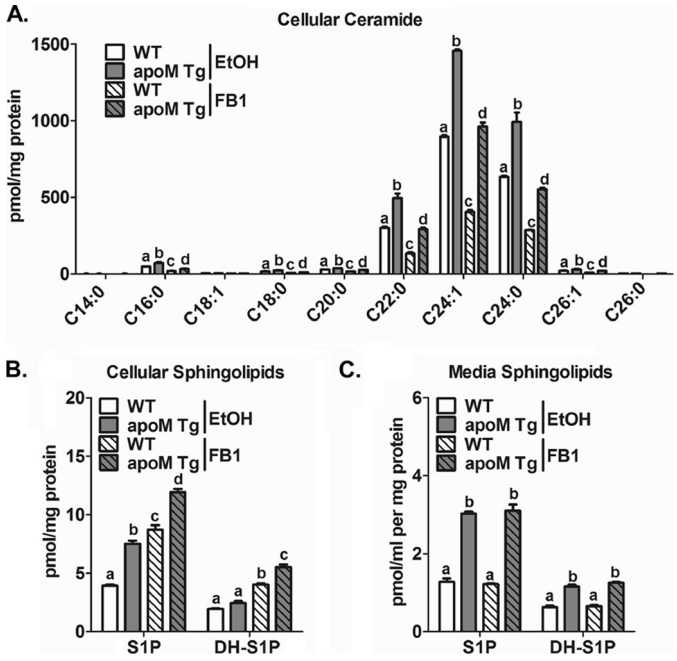


FIGURE 11. **Inhibition of hepatocyte ceramide synthases in *APOM Tg* mice increases cellular levels of S1P and DH-S1P without affecting their secretion.** Primary hepatocytes were isolated from WT and *APOM Tg* mice and treated with vehicle or 25 $\mu$M fumonisin B1 for 6 h in 1 ml of serum-free media. Lipids were extracted from hepatocytes (*A* and *B*) and media (*C*) and the indicated sphingolipids determined by LC-ESI-MS/MS. *A,* different chain length species of ceramide are shown; *numbers* indicate chain length, followed by the number of double bonds in the fatty acid. *Unlike letters* in the figure indicate significant differences ($p < 0.05$) between genotypes or between vehicle and myriocin treatment.

## DISCUSSION

ApoM is a low abundance apolipoprotein that associates with ~5% of plasma HDL particles (13) and is suggested to be atheroprotective (17, 18). Although overexpression of apoM in HEK293 cells leads to generation of larger nascent HDLs (21), it is unclear whether *in vivo* hepatic overexpression of apoM increases HDL particle size. Here, we show that liver-specific human apoM transgenic mice had larger plasma HDL particles that were enriched with CE, LCAT, apoE, apoM, and S1P. Despite the presence of larger plasma HDL particles, *APOM Tg* mice displayed plasma HDL-C concentrations and *in vivo* macrophage reverse cholesterol transport similar to WT mice. Primary hepatocytes from *APOM Tg versus* WT mice generated larger nascent HDL and had increased sphingolipid synthesis and secretion of S1P. Inhibition of ceramide synthase in hepatocytes greatly increased cellular S1P levels, but not secretion, suggesting that apoM is rate-limiting in the export of hepatocyte S1P. Collectively, these data indicate that liver apoM facilitates the generation of larger nascent HDL and stimulates the synthesis and secretion of hepatocyte S1P, both

leading to the presence of large apoM/S1P-enriched plasma HDL. These unique HDL particles may serve to deliver S1P to extrahepatic tissues for atheroprotection or other as yet unidentified functions.

*ApoM Expression and HDL Particle Size*—The appearance of the unique HDL particle enriched in CE, LCAT, apoE, apoM, and S1P in *APOM Tg* mice was observed in both WT and hA-I backgrounds and in the absence of any detectable increase in plasma HDL-C concentrations. In contrast, Christoffersen *et al.* (18) reported that transgenic mice with 10-fold overexpression of apoM had a 13–22% increase in HDL-C compared with WT mice, but HDL particle size was unaffected. In mice deficient in hepatic nuclear factor α or treated with apoM siRNA, both of which result in low apoM expression, HDL particles were larger than their control counterparts (17). However, this phenotype was not confirmed in later studies using apoM knock-out mice (18). The discrepancy regarding HDL particle size between our study and the study by Christoffersen *et al.* (18) may be related to the sensitivity of methods used to detect HDL size changes and differences in *APOM Tg* mouse lines (liver-specific promoter *versus* endogenous promoter). Very recently, another study was published showing that adenoviral overexpression of apoM in mice resulted in larger plasma HDL (23). Here, we show that apoM was predominantly associated with larger sized HDL both in *APOM Tg* mice and WT mice, suggesting that large plasma HDL particles are optimal for binding of apoM and S1P regardless of the level of hepatic apoM expression. In contrast to our results in mice, a study by Lee *et al.* (61) suggested that human plasma S1P was more concentrated in smaller sized $HDL_3$ compared with larger sized $HDL_2$ and that $HDL_3$-S1P is more biologically active in stimulating plasminogen activator inhibitor-1 release from adipocytes than $HDL_2$-S1P. Although Lee *et al.* (61) did not analyze apoM levels, apoM distribution on HDL particles was likely similar to that of S1P, suggesting that apoM is associated with small-sized HDL in human plasma. Differences between our mouse study and the human study could be attributable to cholesteryl ester transfer protein remodeling of human HDL. Cholesteryl ester transfer protein, which is present in human, but not mouse plasma, exchanges CE in HDL for TG in VLDL and LDL, resulting in TG-enriched HDL particles that are substrates for hepatic lipase and endothelial lipase-mediated remodeling to smaller HDL (62). This process may lead to the conversion of large S1P-containing HDL to smaller S1P-containing HDL. Additional studies will be necessary to define the compositional elements of HDL that dictate optimal apoM/S1P binding.

*ApoM and Nascent HDL Formation*—Primary hepatocytes from *APOM Tg* mice generated larger nascent HDL particles compared with hepatocytes from WT mice, agreeing with previous findings that apoM overexpression in ABCA1-expressing HEK293 cells leads to formation of larger nascent HDL (21). After secretion, nascent HDL particles undergo maturation by several lipid transfer proteins and modifying enzymes. LCAT converts FC to CE in HDL, generating spherical HDL particles (9). It is likely the larger nascent HDL particles secreted by *APOM Tg* mouse hepatocytes are the precursor particles for the large plasma HDL particles that are enriched in CE, LCAT, apoE, and apoM/S1P (Fig. 3 and Table 1). Christoffersen *et al.* (18) also observed an increase in HDL apoE content in *APOM Tg* mice, although HDL size and LCAT activity remained unchanged. The LCAT enrichment of HDL likely resulted in increased generation of CE that would help drive HDL particle enlargement, which, in turn, may allow more efficient apoE binding. Previous studies showed that HDL enrichment with SM decreased LCAT-mediated CE formation (63). Consistent with this finding, hepatocyte medium from *APOM Tg* mice had decreased SM concentrations (Fig. 9*C*). These combined results are compatible with the hypothesis that ABCA1-mediated nascent HDL particle assembly in the presence of apoM overexpression results in decreased SM, which in turn allows for more efficient LCAT-mediated cholesterol esterification and HDL particle maturation to larger spherical plasma HDL enriched in apoM/S1P.

*ApoM Overexpression Increases Liver and Hepatocyte S1P Synthesis and Secretion*—S1P is rapidly turned over in plasma ($t_{½}$ ~15 min), suggesting that a high capacity biosynthetic source of S1P is necessary to maintain plasma S1P concentrations (28). Previous studies have suggested that erythrocytes, platelets, and vascular endothelial cells are major contributors to plasma S1P. Platelets have high sphingosine kinase activity and no S1P lyase or phosphatase activity, resulting in a high cellular content of S1P (29, 30). However, a mouse model with virtually no circulating platelets had normal plasma S1P levels, suggesting the existence of other cellular sources of plasma S1P (27). Results from adoptive transplantation of WT bone marrow into mice without plasma S1P due to conditional ablation of SphK1 and SphK2 demonstrated that hematopoietic cells are a major source of plasma S1P (27). Furthermore, using mice with deletion of SphK1 and SphK2 in hematopoietic cells, it was conclusively demonstrated that erythrocytes are a major source of plasma S1P (27). Surprisingly, however, mice that were thrombocytopenic, anemic, or leukopenic did not show an appreciable reduction in plasma S1P, again indicating the existence of other tissue sources of S1P (28). Adenoviral overexpression of SphK1 in livers of SphK1 whole body knock-out mice restored plasma S1P levels, which was attributed to enhanced secretion of S1P from liver endothelial cells, not hepatocytes, because cultured endothelial cells secreted more S1P than primary hepatocytes (28). However, because there are many more hepatocytes than endothelial cells in liver, this conclusion may have been premature. In this study, we show that hepatocytes secrete significant amounts of S1P and DH-S1P and that overexpression of apoM enhances their secretion. Furthermore, apoM, the major carrier for plasma S1P (22), is mostly expressed in the liver and kidney, and its expression levels directly correlate with levels of plasma S1P (22), as well as its secretion from hepatocytes (Figs. 8, 10, and 11). Hence, it appears, based on this study and other evidence, that hepatocytes are an important source of plasma S1P.

Our data suggest that in addition to its role in maintaining plasma S1P levels and as a carrier of intravascular S1P to extrahepatic tissues, apoM also stimulates hepatic S1P production. Interestingly, apoM overexpression in hepatocytes also enhanced levels of ceramide, most likely resulting from enhancement of the salvage/recycling pathway, because inhibition of ceramide synthases

with FB1, but not inhibition of *de novo* sphingolipid synthesis with myriocin, reduced ceramide elevations. Although FB1 treatment increased cellular S1P and DH-S1P, it did not affect their secretion (Fig. 11), suggesting that hepatocyte apoM production is rate-limiting in S1P secretion.

*Hepatic Sphingolipid Production and Cholesterol Metabolism*—Hepatocytes from *APOM Tg* mice had increased cellular ceramide and SM content (Fig. 9) and secreted larger nascent HDL particles (Fig. 5), suggesting that there is coordination between sphingolipid and cholesterol metabolism. Sphingolipids and cholesterol not only serve as essential structural components of membranes, especially lipid microdomains (64), but also regulate the metabolism of one another. For example, induction of cellular sphingolipid storage stimulated cholesterol synthesis by activating sterol-responsive element-binding protein 2 (SREBP2), a major transcriptional regulator of genes involved in cholesterol uptake and biosynthesis. Conversely, sphingomyelin depletion inhibited SREBP2 activation (65), resulting in cholesterol synthesis inhibition (66). Ceramide treatment of nonhepatic cell lines also promoted ABCA1-mediated cholesterol efflux (67). In mice deficient in S1P lyase, an enzyme responsible for S1P degradation, plasma HDL-C and LDL-C were significantly increased, as were plasma and liver S1P (68), suggesting a sphingolipid intermediate or S1P may regulate HDL and LDL production. These data support the hypothesis that increased hepatocyte ceramide, sphingomyelin, and/or S1P content in *APOM Tg* mice may contribute to the generation of larger nascent HDLs.

In conclusion, our study demonstrates that hepatocyte-specific apoM overexpression facilitates formation of large apoM/S1P-enriched HDL by promoting formation of large nascent HDL and stimulating sphingolipid synthesis and S1P secretion. These unique HDL particles may serve to deliver S1P to extrahepatic tissues for atheroprotection or other functions.

*Acknowledgments—We gratefully acknowledge Karen Klein (Translational Science Institute, Wake Forest School of Medicine) for editing the manuscript. LDL receptor-related protein antibody was generously provided by Dr. Joachim Herz (University of Texas Southwestern Medical Center), and ldlA-SR-BI-expressing cells were generously provided by Dr. Monty Krieger (Massachusetts Institute of Technology). Mass spectrometry analyses in Fig. 6 were performed at the Mass Spectrometer Facility, Comprehensive Cancer Center, Wake Forest University, and were supported, in part, by National Institutes of Health NCI Center Grant 5P30CA12197. The TSQ Discovery Max LC-MS/MS was acquired through a North Carolina Biotechnology Center Grant 2007-IDG-1021 (to M. J. T.). Sphingolipid analyses were performed at the Lipidomics Facility, Department of Biochemistry and Molecular Biology, Virginia Commonwealth University School of Medicine, and were supported, in part, by funding to the Massey Cancer Center from National Institutes of Health NCI Cancer Center Support Grant P30 CA016059.*

## REFERENCES

1. Fisher, E. A., Feig, J. E., Hewing, B., Hazen, S. L., and Smith, J. D. (2012) High-density lipoprotein function, dysfunction, and reverse cholesterol transport. *Arterioscler. Thromb. Vasc. Biol.* **32,** 2813–2820
2. AIM-HIGH Investigators, Boden, W. E., Probstfield, J. L., Anderson, T., Chaitman, B. R., Desvignes-Nickens, P., Koprowicz, K., McBride, R., Teo, K., and Weintraub, W. (2011) Niacin in patients with low HDL cholesterol levels receiving intensive statin therapy. *N. Engl. J. Med.* **365,** 2255–2267
3. Voight, B. F., Peloso, G. M., Orho-Melander, M., Frikke-Schmidt, R., Barbalic, M., Jensen, M. K., Hindy, G., Hólm, H., Ding, E. L., Johnson, T., Schunkert, H., Samani, N. J., Clarke, R., Hopewell, J. C., Thompson, J. F., Li, M., Thorleifsson, G., Newton-Cheh, C., Musunuru, K., Pirruccello, J. P., Saleheen, D., Chen, L., Stewart, A., Schillert, A., Thorsteinsdottir, U., Thorgeirsson, G., Anand, S., Engert, J. C., Morgan, T., Spertus, J., Stoll, M., Berger, K., Martinelli, N., Girelli, D., McKeown, P. P., Patterson, C. C., Epstein, S. E., Devaney, J., Burnett, M. S., Mooser, V., Ripatti, S., Surakka, I., Nieminen, M. S., Sinisalo, J., Lokki, M. L., Perola, M., Havulinna, A., de Faire, U., Gigante, B., Ingelsson, E., Zeller, T., Wild, P., de Bakker, P. I., Klungel, O. H., Maitland-van der Zee, A. H., Peters, B. J., de Boer, A., Grobbee, D. E., Kamphuisen, P. W., Deneer, V. H., Elbers, C. C., Onland-Moret, N. C., Hofker, M. H., Wijmenga, C., Verschuren, W. M., Boer, J. M., van der Schouw, Y. T., Rasheed, A., Frossard, P., Demissie, S., Willer, C., Do, R., Ordovas, J. M., Abecasis, G. R., Boehnke, M., Mohlke, K. L., Daly, M. J., Guiducci, C., Burtt, N. P., Surti, A., Gonzalez, E., Purcell, S., Gabriel, S., Marrugat, J., Peden, J., Erdmann, J., Diemert, P., Willenborg, C., König, I. R., Fischer, M., Hengstenberg, C., Ziegler, A., Buysschaert, I., Lambrechts, D., Van de Werf, F., Fox, K. A., El Mokhtari, N. E., Rubin, D., Schrezenmeir, J., Schreiber, S., Schäfer, A., Danesh, J., Blankenberg, S., Roberts, R., McPherson, R., Watkins, H., Hall, A. S., Overvad, K., Rimm, E., Boerwinkle, E., Tybjaerg-Hansen, A., Cupples, L. A., Reilly, M. P., Melander, O., Mannucci, P. M., Ardissino, D., Siscovick, D., Elosua, R., Stefansson, K., O'Donnell, C. J., Salomaa, V., Rader, D. J., Peltonen, L., Schwartz, S. M., Altshuler, D., and Kathiresan, S. (2012) Plasma HDL cholesterol and risk of myocardial infarction: a mendelian randomisation study. *Lancet* **380,** 572–580
4. Glomset, J. A. (1968) The plasma lecithins:cholesterol acyltransferase reaction. *J. Lipid Res.* **9,** 155–167
5. Mineo, C., and Shaul, P. W. (2012) Novel biological functions of high-density lipoprotein cholesterol. *Circ. Res.* **111,** 1079–1090
6. Barter, P. J., Nicholls, S., Rye, K. A., Anantharamaiah, G. M., Navab, M., and Fogelman, A. M. (2004) Anti-inflammatory properties of HDL. *Circ. Res.* **95,** 764–772
7. Nofer, J. R. (2008) High-density lipoprotein, sphingosine 1-phosphate, and atherosclerosis. *J. Clin. Lipidol.* **2,** 4–11
8. Timmins, J. M., Lee, J. Y., Boudyguina, E., Kluckman, K. D., Brunham, L. R., Mulya, A., Gebre, A. K., Coutinho, J. M., Colvin, P. L., Smith, T. L., Hayden, M. R., Maeda, N., and Parks, J. S. (2005) Targeted inactivation of hepatic Abca1 causes profound hypoalphalipoproteinemia and kidney hypercatabolism of apoA-I. *J. Clin. Invest.* **115,** 1333–1342
9. Santamarina-Fojo, S., Lambert, G., Hoeg, J. M., and Brewer, H. B., Jr. (2000) Lecithin-cholesterol acyltransferase: role in lipoprotein metabolism, reverse cholesterol transport and atherosclerosis. *Curr. Opin. Lipidol.* **11,** 267–275
10. Yazdanyar, A., Yeang, C., and Jiang, X. C. (2011) Role of phospholipid transfer protein in high-density lipoprotein-mediated reverse cholesterol transport. *Curr. Atheroscler. Rep.* **13,** 242–248
11. Brundert, M., Ewert, A., Heeren, J., Behrendt, B., Ramakrishnan, R., Greten, H., Merkel, M., and Rinninger, F. (2005) Scavenger receptor class B type I mediates the selective uptake of high-density lipoprotein-associated cholesteryl ester by the liver in mice. *Arterioscler. Thromb. Vasc. Biol.* **25,** 143–148
12. Ahnström, J., Faber, K., Axler, O., and Dahlbäck, B. (2007) Hydrophobic ligand binding properties of the human lipocalin apolipoprotein M. *J. Lipid Res.* **48,** 1754–1762
13. Xu, N., and Dahlbäck, B. (1999) A novel human apolipoprotein (apoM). *J. Biol. Chem.* **274,** 31286–31290
14. Nielsen, L. B., Christoffersen, C., Ahnström, J., and Dahlbäck, B. (2009) ApoM: gene regulation and effects on HDL metabolism. *Trends Endocrinol. Metab.* **20,** 66–71
15. Dahlbäck, B., and Nielsen, L. B. (2009) Apolipoprotein M affecting lipid metabolism or just catching a ride with lipoproteins in the circulation? *Cell. Mol. Life Sci.* **66,** 559–564
16. Christoffersen, C., Ahnström, J., Axler, O., Christensen, E. I., Dahlbäck, B., and Nielsen, L. B. (2008) The signal peptide anchors apolipoprotein M in

plasma lipoproteins and prevents rapid clearance of apolipoprotein M from plasma. *J. Biol. Chem.* **283,** 18765–18772
17. Wolfrum, C., Poy, M. N., and Stoffel, M. (2005) Apolipoprotein M is required for preβ-HDL formation and cholesterol efflux to HDL and protects against atherosclerosis. *Nat. Med.* **11,** 418–422
18. Christoffersen, C., Jauhiainen, M., Moser, M., Porse, B., Ehnholm, C., Boesl, M., Dahlbäck, B., and Nielsen, L. B. (2008) Effect of apolipoprotein M on high density lipoprotein metabolism and atherosclerosis in low density lipoprotein receptor knock-out mice. *J. Biol. Chem.* **283,** 1839–1847
19. Elsoe, S., Christoffersen, C., Luchoomun, J., Turner, S., and Nielsen, L. B. (2013) Apolipoprotein M promotes mobilization of cellular cholesterol *in vivo*. *Biochim. Biophys. Acta* **1831,** 1287–1292
20. Elsøe, S., Ahnström, J., Christoffersen, C., Hoofnagle, A. N., Plomgaard, P., Heinecke, J. W., Binder, C. J., Björkbacka, H., Dahlbäck, B., and Nielsen, L. B. (2012) Apolipoprotein M binds oxidized phospholipids and increases the antioxidant effect of HDL. *Atherosclerosis* **221,** 91–97
21. Mulya, A., Seo, J., Brown, A. L., Gebre, A. K., Boudyguina, E., Shelness, G. S., and Parks, J. S. (2010) Apolipoprotein M expression increases the size of nascent preβ HDL formed by ATP binding cassette transporter A1. *J. Lipid Res.* **51,** 514–524
22. Christoffersen, C., Obinata, H., Kumaraswamy, S. B., Galvani, S., Ahnström, J., Sevvana, M., Egerer-Sieber, C., Muller, Y. A., Hla, T., Nielsen, L. B., and Dahlbäck, B. (2011) Endothelium-protective sphingosine 1-phosphate provided by HDL-associated apolipoprotein M. *Proc. Natl. Acad. Sci. U.S.A.* **108,** 9613–9618
23. Kurano, M., Tsukamoto, K., Ohkawa, R., Hara, M., Iino, J., Kageyama, Y., Ikeda, H., and Yatomi, Y. (2013) Liver involvement in sphingosine 1-phosphate dynamism revealed by adenoviral hepatic overexpression of apolipoprotein M. *Atherosclerosis* **229,** 102–109
24. Wilkerson, B. A., Grass, G. D., Wing, S. B., Argraves, W. S., and Argraves, K. M. (2012) Sphingosine 1-phosphate (S1P) carrier-dependent regulation of endothelial barrier: high density lipoprotein (HDL)-S1P prolongs endothelial barrier enhancement as compared with albumin-S1P via effects on levels, trafficking, and signaling of S1P1. *J. Biol. Chem.* **287,** 44645–44653
25. Obinata, H., and Hla, T. (2012) Sphingosine 1-phosphate in coagulation and inflammation. *Semin. Immunopathol.* **34,** 73–91
26. Egom, E. E., Mamas, M. A., and Soran, H. (2013) HDL quality or cholesterol cargo: what really matters–spotlight on sphingosine 1-phosphate-rich HDL. *Curr. Opin. Lipidol.* **24,** 351–356
27. Pappu, R., Schwab, S. R., Cornelissen, I., Pereira, J. P., Regard, J. B., Xu, Y., Camerer, E., Zheng, Y. W., Huang, Y., Cyster, J. G., and Coughlin, S. R. (2007) Promotion of lymphocyte egress into blood and lymph by distinct sources of sphingosine 1-phosphate. *Science* **316,** 295–298
28. Venkataraman, K., Lee, Y. M., Michaud, J., Thangada, S., Ai, Y., Bonkovsky, H. L., Parikh, N. S., Habrukowich, C., and Hla, T. (2008) Vascular endothelium as a contributor of plasma sphingosine 1-phosphate. *Circ. Res.* **102,** 669–676
29. English, D., Welch, Z., Kovala, A. T., Harvey, K., Volpert, O. V., Brindley, D. N., and Garcia, J. G. (2000) Sphingosine 1-phosphate released from platelets during clotting accounts for the potent endothelial cell chemotactic activity of blood serum and provides a novel link between hemostasis and angiogenesis. *FASEB J.* **14,** 2255–2265
30. Yatomi, Y., Igarashi, Y., Yang, L., Hisano, N., Qi, R., Asazuma, N., Satoh, K., Ozaki, Y., and Kume, S. (1997) Sphingosine 1-phosphate, a bioactive sphingolipid abundantly stored in platelets, is a normal constituent of human plasma and serum. *J. Biochem.* **121,** 969–973
31. Simonet, W. S., Bucay, N., Lauer, S. J., and Taylor, J. M. (1993) A far-downstream hepatocyte-specific control region directs expression of the linked human apolipoprotein E and C-I genes in transgenic mice. *J. Biol. Chem.* **268,** 8221–8229
32. Engelking, L. J., Kuriyama, H., Hammer, R. E., Horton, J. D., Brown, M. S., Goldstein, J. L., and Liang, G. (2004) Overexpression of Insig-1 in the livers of transgenic mice inhibits SREBP processing and reduces insulin-stimulated lipogenesis. *J. Clin. Invest.* **113,** 1168–1175
33. Temel, R. E., Tang, W., Ma, Y., Rudel, L. L., Willingham, M. C., Ioannou, Y. A., Davies, J. P., Nilsson, L. M., and Yu, L. (2007) Hepatic Niemann-Pick C1-like 1 regulates biliary cholesterol concentration and is a target of ezetimibe. *J. Clin. Invest.* **117,** 1968–1978
34. Vaisman, B. L., Lambert, G., Amar, M., Joyce, C., Ito, T., Shamburek, R. D., Cain, W. J., Fruchart-Najib, J., Neufeld, E. D., Remaley, A. T., and Brewer, H. B., Jr., and Santamarina-Fojo, S. (2001) ABCA1 overexpression leads to hyperalphalipoproteinemia and increased biliary cholesterol excretion in transgenic mice. *J. Clin. Invest.* **108,** 303–309
35. Brown, J. M., Bell, T. A., 3rd, Alger, H. M., Sawyer, J. K., Smith, T. L., Kelley, K., Shah, R., Wilson, M. D., Davis, M. A., Lee, R. G., Graham, M. J., Crooke, R. M., and Rudel, L. L. (2008) Targeted depletion of hepatic ACAT2-driven cholesterol esterification reveals a non-biliary route for fecal neutral sterol loss. *J. Biol. Chem.* **283,** 10522–10534
36. Carr, T. P., Parks, J. S., and Rudel, L. L. (1992) Hepatic ACAT activity in African green monkeys is highly correlated to plasma LDL cholesteryl ester enrichment and coronary artery atherosclerosis. *Arterioscler. Thromb.* **12,** 1274–1283
37. Carr, T. P., Andresen, C. J., and Rudel, L. L. (1993) Enzymatic determination of triglyceride, free cholesterol, and total cholesterol in tissue lipid extracts. *Clin. Biochem.* **26,** 39–42
38. Koritnik, D. L., and Rudel, L. L. (1983) Measurement of apolipoprotein A-I concentration in nonhuman primate serum by enzyme-linked immunosorbent assay (ELISA). *J. Lipid Res.* **24,** 1639–1645
39. Naik, S. U., Wang, X., Da Silva, J. S., Jaye, M., Macphee, C. H., Reilly, M. P., Billheimer, J. T., Rothblat, G. H., and Rader, D. J. (2006) Pharmacological activation of liver X receptors promotes reverse cholesterol transport *in vivo*. *Circulation* **113,** 90–97
40. Temel, R. E., Sawyer, J. K., Yu, L., Lord, C., Degirolamo, C., McDaniel, A., Marshall, S., Wang, N., Shah, R., Rudel, L. L., and Brown, J. M. (2010) Biliary sterol secretion is not required for macrophage reverse cholesterol transport. *Cell Metab.* **12,** 96–102
41. Millar, J. S., Cromley, D. A., McCoy, M. G., Rader, D. J., and Billheimer, J. T. (2005) Determining hepatic triglyceride production in mice: comparison of poloxamer 407 with Triton WR-1339. *J. Lipid Res.* **46,** 2023–2028
42. Chung, S., Timmins, J. M., Duong, M., Degirolamo, C., Rong, S., Sawyer, J. K., Singaraja, R. R., Hayden, M. R., Maeda, N., Rudel, L. L., Shelness, G. S., and Parks, J. S. (2010) Targeted deletion of hepatocyte ABCA1 leads to very low density lipoprotein triglyceride overproduction and low density lipoprotein hypercatabolism. *J. Biol. Chem.* **285,** 12197–12209
43. Mulya, A., Lee, J. Y., Gebre, A. K., Thomas, M. J., Colvin, P. L., and Parks, J. S. (2007) Minimal lipidation of pre-β HDL by ABCA1 results in reduced ability to interact with ABCA1. *Arterioscler. Thromb. Vasc. Biol.* **27,** 1828–1836
44. Hait, N. C., Allegood, J., Maceyka, M., Strub, G. M., Harikumar, K. B., Singh, S. K., Luo, C., Marmorstein, R., Kordula, T., Milstien, S., and Spiegel, S. (2009) Regulation of histone acetylation in the nucleus by sphingosine 1-phosphate. *Science* **325,** 1254–1257
45. Berdyshev, E. V., Gorshkova, I. A., Garcia, J. G., Natarajan, V., and Hubbard, W. C. (2005) Quantitative analysis of sphingoid base-1-phosphates as bisacetylated derivatives by liquid chromatography-tandem mass spectrometry. *Anal. Biochem.* **339,** 129–136
46. Maceyka, M., Sankala, H., Hait, N. C., Le Stunff, H., Liu, H., Toman, R., Collier, C., Zhang, M., Satin, L. S., Merrill, A. H., Jr., Milstien, S., and Spiegel, S. (2005) SphK1 and SphK2, sphingosine kinase isoenzymes with opposing functions in sphingolipid metabolism. *J. Biol. Chem.* **280,** 37118–37129
47. Mitra, P., Payne, S. G., Milstien, S., and Spiegel, S. (2007) A rapid and sensitive method to measure secretion of sphingosine 1-phosphate. *Methods Enzymol.* **434,** 257–264
48. Fiske, C. H., and Subbarow, Y. (1925) The colorimetric determination of phosphorus. *J. Biol. Chem.* **66,** 375–400
49. Livak, K. J., and Schmittgen, T. D. (2001) Analysis of relative gene expression data using real-time quantitative PCR and the $2(-\Delta\Delta C(T))$ method. *Methods* **25,** 402–408
50. Rubin, E. M., Ishida, B. Y., Clift, S. M., and Krauss, R. M. (1991) Expression of human apolipoprotein A-I in transgenic mice results in reduced plasma levels of murine apolipoprotein A-I and the appearance of two new high density lipoprotein size subclasses. *Proc. Natl. Acad. Sci. U.S.A.* **88,** 434–438
51. Christoffersen, C., Pedersen, T. X., Gordts, P. L., Roebroek, A. J., Dahlbäck,

B., and Nielsen, L. B. (2010) Opposing effects of apolipoprotein M on catabolism of apolipoprotein B-containing lipoproteins and atherosclerosis. *Circ. Res.* **106,** 1624–1634
52. Jiang, X. C., Beyer, T. P., Li, Z., Liu, J., Quan, W., Schmidt, R. J., Zhang, Y., Bensch, W. R., Eacho, P. I., and Cao, G. (2003) Enlargement of high density lipoprotein in mice via liver X receptor activation requires apolipoprotein E and is abolished by cholesteryl ester transfer protein expression. *J. Biol. Chem.* **278,** 49072–49078
53. Vassiliou, G., and McPherson, R. (2004) A novel efflux-recapture process underlies the mechanism of high-density lipoprotein cholesteryl ester-selective uptake mediated by the low-density lipoprotein receptor-related protein. *Arterioscler. Thromb. Vasc. Biol.* **24,** 1669–1675
54. Vassiliou, G., Benoist, F., Lau, P., Kavaslar, G. N., and McPherson, R. (2001) The low density lipoprotein receptor-related protein contributes to selective uptake of high density lipoprotein cholesteryl esters by SW872 liposarcoma cells and primary human adipocytes. *J. Biol. Chem.* **276,** 48823–48830
55. Varban, M. L., Rinninger, F., Wang, N., Fairchild-Huntress, V., Dunmore, J. H., Fang, Q., Gosselin, M. L., Dixon, K. L., Deeds, J. D., Acton, S. L., Tall, A. R., and Huszar, D. (1998) Targeted mutation reveals a central role for SR-BI in hepatic selective uptake of high density lipoprotein cholesterol. *Proc. Natl. Acad. Sci. U.S.A.* **95,** 4619–4624
56. Acton, S., Rigotti, A., Landschulz, K. T., Xu, S., Hobbs, H. H., and Krieger, M. (1996) Identification of scavenger receptor SR-BI as a high density lipoprotein receptor. *Science* **271,** 518–520
57. Karuna, R., Park, R., Othman, A., Holleboom, A. G., Motazacker, M. M., Sutter, I., Kuivenhoven, J. A., Rohrer, L., Matile, H., Hornemann, T., Stoffel, M., Rentsch, K. M., and von Eckardstein, A. (2011) Plasma levels of sphingosine 1-phosphate and apolipoprotein M in patients with monogenic disorders of HDL metabolism. *Atherosclerosis* **219,** 855–863
58. Miyake, Y., Kozutsumi, Y., Nakamura, S., Fujita, T., and Kawasaki, T. (1995) Serine palmitoyltransferase is the primary target of a sphingosine-like immunosuppressant, ISP-1/myriocin. *Biochem. Biophys. Res. Commun.* **211,** 396–403
59. Wang, E., Norred, W. P., Bacon, C. W., Riley, R. T., and Merrill, A. H., Jr. (1991) Inhibition of sphingolipid biosynthesis by fumonisins. Implications for diseases associated with *Fusarium moniliforme*. *J. Biol. Chem.* **266,** 14486–14490
60. Mullen, T. D., Jenkins, R. W., Clarke, C. J., Bielawski, J., Hannun, Y. A., and Obeid, L. M. (2011) Ceramide synthase-dependent ceramide generation and programmed cell death: involvement of salvage pathway in regulating postmitochondrial events. *J. Biol. Chem.* **286,** 15929–15942
61. Lee, M. H., Hammad, S. M., Semler, A. J., Luttrell, L. M., Lopes-Virella, M. F., and Klein, R. L. (2010) HDL3, but not HDL2, stimulates plasminogen activator inhibitor-1 release from adipocytes: the role of sphingosine 1-phosphate. *J. Lipid Res.* **51,** 2619–2628
62. Barter, P. J., Hopkins, G. J., and Calvert, G. D. (1982) Transfers and exchanges of esterified cholesterol between plasma lipoproteins. *Biochem. J.* **208,** 1–7
63. Subbaiah, P. V., and Liu, M. (1993) Role of sphingomyelin in the regulation of cholesterol esterification in the plasma lipoproteins. Inhibition of lecithin-cholesterol acyltransferase reaction. *J. Biol. Chem.* **268,** 20156–20163
64. Lingwood, D., and Simons, K. (2010) Lipid rafts as a membrane-organizing principle. *Science* **327,** 46–50
65. Puri, V., Jefferson, J. R., Singh, R. D., Wheatley, C. L., Marks, D. L., and Pagano, R. E. (2003) Sphingolipid storage induces accumulation of intracellular cholesterol by stimulating SREBP-1 cleavage. *J. Biol. Chem.* **278,** 20961–20970
66. Scheek, S., Brown, M. S., and Goldstein, J. L. (1997) Sphingomyelin depletion in cultured cells blocks proteolysis of sterol regulatory element binding proteins at site 1. *Proc. Natl. Acad. Sci. U.S.A.* **94,** 11179–11183
67. Witting, S. R., Maiorano, J. N., and Davidson, W. S. (2003) Ceramide enhances cholesterol efflux to apolipoprotein A-I by increasing the cell surface presence of ATP-binding cassette transporter A1. *J. Biol. Chem.* **278,** 40121–40127
68. Bektas, M., Allende, M. L., Lee, B. G., Chen, W., Amar, M. J., Remaley, A. T., Saba, J. D., and Proia, R. L. (2010) Sphingosine 1-phosphate lyase deficiency disrupts lipid homeostasis in liver. *J. Biol. Chem.* **285,** 10880–10889